Effect of grain size distribution on the development of compaction localization in porous sandstone

Cecilia Cheung, Patrick Baud, Teng-Fong Wong

Effect of grain size distribution on the development of compaction localization in porous sandstone

Cecilia S. N. Cheung,[1] Patrick Baud,[2] and Teng-fong Wong[1]

Received 11 September 2012; revised 30 September 2012; accepted 4 October 2012; published 6 November 2012.

[1] Compaction bands are strain localization structures that are relatively impermeable and can act as barriers to fluid flow in reservoirs. Laboratory studies have shown that discrete compaction bands develop in several sandstones with porosities of 22–25%, at stress states in the transitional regime between brittle faulting and cataclastic flow. To identify the microstructural parameters that influence compaction band formation, we conducted a systematic study of mechanical deformation, failure mode and microstructural evolution in Bleurswiller and Boise sandstones, of similar porosity (~25%) and mineralogy but different sorting. Discrete compaction bands were observed to develop over a wide range of pressure in the Bleurswiller sandstone that has a relatively uniform grain size distribution. In contrast, compaction localization was not observed in the poorly sorted Boise sandstone. Our results demonstrate that grain size distribution exerts important influence on compaction band development, in agreement with recently published data from Valley of Fire and Buckskin Gulch, as well as numerical studies. **Citation:** Cheung, C. S. N., P. Baud, and T. Wong (2012), Effect of grain size distribution on the development of compaction localization in porous sandstone, *Geophys. Res. Lett.*, *39*, L21302, doi:10.1029/2012GL053739.

1. Introduction

[2] Structural discontinuities such as fracture and deformation band are pervasive in the Earth's crust. They have profound influence on the extraction of petroleum from reservoirs, structural integrity of repositories, and potential leakage of sequestered CO_2 and disposed waste. One end entity of deformation band is compaction band, a thin tabular structure with inelastic compaction in direction subperpendicular to its planar surface without evident shear offset [*Aydin et al.*, 2006].

[3] Since the seminal study of *Mollema and Antonellini* [1996], a number of field, laboratory and numerical studies have been conducted to characterize compaction bands and probe the mechanics of compaction localization. Most observations have been on porous sandstone, and an intriguing question remains unanswered: why have compaction bands been observed in only some sandstones but not the others? The answer would probably hinge on a fundamental understanding of the mechanics and how petrophysical attributes inhibit or promote compaction band formation. Previous laboratory studies have documented the development of discrete compaction bands and permeability evolution in three sandstones with porosities ranging from 22 to 25% [*Klein et al.*, 2001; *Wong et al.*, 2001; *Baud et al.*, 2004; *Vajdova et al.*, 2004; *Fortin et al.*, 2006; *Baud et al.*, 2012]. Recent field observations of compaction bands that include detailed microstructural characterization [*Eichhubl et al.*, 2010; *Schultz et al.*, 2010; *Fossen et al.*, 2011] also indicate that the sandstones in these formations are well sorted. Furthermore, numerical simulations using network [*Katsman et al.*, 2005] and discrete element [*Wang et al.*, 2008] modeling have shown that compaction bands preferentially developed in an assembly that has a relatively uniform grain size distribution. Hence, these field and numerical studies suggest that, in addition to porosity, sorting is also an important petrophysical attribute that influences compaction band formation. To compare and possibly validate these observations, we conducted a systematic laboratory study of a pair of well and poorly sorted porous sandstones with similar mineralogy and porosity, with the objective of elucidating the micromechanical processes by which grain size distribution may control the mode of compaction localization.

2. Field and Laboratory Observations of Compaction Bands

[4] Compaction bands have been widely observed in two field areas: Aztec sandstone at Valley of Fire State Park, Nevada [*Hill*, 1989], and Navajo sandstone at Buckskin Gulch adjacent to the East Kaibab monocline, Utah [*Mollema and Antonellini*, 1996]. These bands have thicknesses and trace lengths on the order of 1–10 mm and 1–10 m, respectively [*Sternlof et al.*, 2005].

[5] Recent investigation of compaction bands in these two areas has incorporated systematic microstructural characterization, which allows us to determine the grain size distributions. We analyzed the micrographs in Figure 9b of *Eichhubl et al.* [2010] and Figure S1 (layers 2 and 4) of *Schultz et al.* [2010] that are associated with pure compaction bands in Aztec and Navajo sandstones, respectively. A thresholding technique was used to binarize the micrographs, such that individual grains can be identified. The equivalent diameter of a circle with the same area as a grain was evaluated. It can be seen from Figure 1c that the grain size distributions of pure compaction bands in both field areas span over a relatively narrow range of ~300 μm.

[6] Laboratory studies under controlled stress conditions have provided useful insights into the mechanics of compaction band formation. Discrete compaction bands (with

[1]Department of Geosciences, State University of New York, Stony Brook, New York, USA.
[2]Institut de Physique du Globe de Strasbourg, UMR 7516 CNRS, EOST, Université de Strasbourg, Strasbourg, France.

Corresponding author: C. S. N. Cheung, Department of Geosciences, State University of New York, Stony Brook, NY 11794-2100, USA. (seengacecilia.cheung@stonybrook.edu)

0094-8276/12/2012GL053739

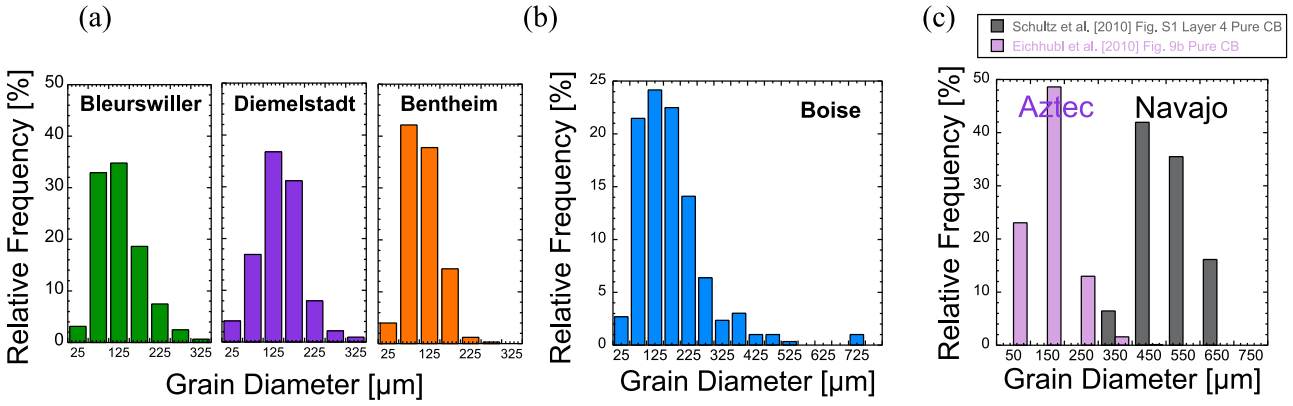

Figure 1. Grain size distributions of (a) Bleurswiller, Diemelstadt and Bentheim sandstones that failed by compaction band formation, (b) Boise sandstone that failed by distributed cataclastic flow (Note the different scale), and (c) Navajo sandstone from Buckskin Gulch and Aztec sandstone from Valley of Fire. Navajo sandstone data are based on Figure S1 of *Schultz et al.* [2010]. We only show data for layer 4, but those for layer 2 are similar. Aztec sandstone data are based on Figure 9b of *Eichhubl et al.* [2010].

thicknesses of ~2–3 grain diameters) have been observed in Bentheim, Diemelstadt and Bleurswiller sandstones, with petrophysical properties as described in Table S1 in the auxiliary material.[1] One of the earliest investigations was on Bentheim sandstone by *Klein et al.* [2001], who speculated that its relatively homogeneous mineralogy and well sorted grains both promote formation of discrete compaction bands. The Aztec and Navajo sandstones, in which compaction bands are observed in the field, are also predominately made up of quartz grains. However, subsequent studies on Diemelstadt and Bleurswiller sandstones have shown that discrete compaction bands can be formed in more complex mineralogy [*Baud et al.*, 2004; *Fortin et al.*, 2006]. These two sandstones are similar to Bentheim sandstone in porosity (Table S1), but possibly due to abundance of minerals other than quartz (feldspar, oxide and mica), their compactive yield stresses are lower by as much as a factor of 5 [*Tembe et al.*, 2008].

[7] In many respects, the morphological attributes of discrete compaction bands as observed in the laboratory are similar to compaction bands in the field. Notwithstanding these similarities, the dimensions (thickness and length) documented in the field are appreciably larger than those in the laboratory deformed samples. It seems that the initiation and development of compaction bands in the field are related to heterogeneities larger than grain scale. The damage intensity and stress level for compaction band formation are also inferred to be lower in the field [*Eichhubl et al.*, 2010; *Fossen et al.*, 2011]. Synthesizing field and laboratory measurements, *Tembe et al.* [2008] observed that both types of data follow an overall trend with the compaction band thickness directly proportional to the square-root of band length.

3. Sandstone and Grain Size Distribution

[8] We selected Bleurswiller and Boise sandstones for a systematic comparison. A detailed petrophysical description is provided in Table S1. We show in Figure 1a the grain size distributions for Bentheim, Diemelstadt and Bleurswiller sandstones which have been documented to develop compaction bands in the laboratory. These three sandstones have relatively narrow grain size distributions that range up to only ~300 μm. Figure 1b shows our data for Boise sandstone, which has a significantly broader distribution with effective grain diameter ranging up to 750 μm. Even though it is similar to Bleurswiller sandstone in mineralogy and porosity, Boise sandstone has a significantly different sorting. The use of histograms can be deceiving since it is sensitive to bin selection. We provide in Figure S2 the corresponding cumulative frequency curves, which corroborate the inferred differences in sorting between Bleurswiller and Boise sandstones.

4. Mechanical Deformation

[9] Mechanical tests were conducted in the conventional triaxial compression configuration, with compressive principal stresses given by $\sigma_1 > \sigma_2 = \sigma_3$. Difference between the confining pressure (P_C) and pore pressure (P_P) will be referred to as effective pressure (P_{eff}). The effective mean stress and differential stress are given by $(\sigma_1 + 2\sigma_3)/3 - P_P$ and $\sigma_1 - \sigma_3$, respectively. The jacketed samples (with a diameter of 18.4 mm and length of 38.1 mm) were saturated with deionized water and deformed at a fixed $P_P = 10$ MPa under fully drained conditions at room temperature. We deformed 9 Boise sandstone samples at P_{eff} ranging from 5–90 MPa, at a servo-controlled axial displacement rate that corresponds to a nominal axial strain rate of 1.3×10^{-5} s^{-1}. A hydrostatic compression experiment was also conducted. The tests followed methodology detailed in *Tembe et al.* [2008].

[10] The differential stress-axial strain curves for 4 Boise sandstone samples are presented in Figure 2a. At $P_{eff} = 5$ MPa, the sample attained a peak stress, beyond which it strain softened with a significant stress drop. At an elevated pressure (≥40 MPa), the stress-strain curve showed monotonic strain hardening. In Figure S1 we plot the effective mean stress as a function of porosity change for 6 samples that failed by cataclastic flow. For reference the hydrostat is also shown, with the inflection point P^*corresponding to the critical pressure for onset of grain crushing and pore

[1]Auxiliary materials are available in the HTML. doi:10.1029/2012GL053739.

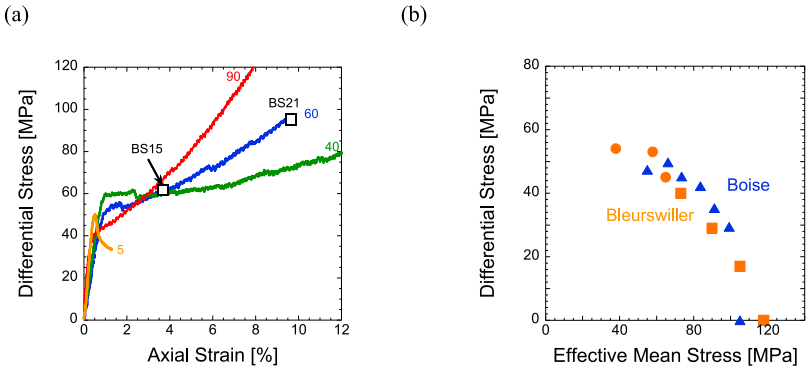

Figure 2. (a) Differential stress versus axial strain for representative triaxial compression experiments on saturated Boise sandstone. The effective pressures in MPa are indicated next to each curve. In this paper, we highlighted the post-mortem microstructural observations on two samples deformed at P_{eff} = 60 MPa, marked by squares. (b) Compactive yield envelope for the onset of shear-enhanced compaction (C^*) and failure modes plotted in the differential versus effective mean stress space for Boise (blue) and Bleurswiller (orange) sandstone. The two sandstones show similar yield strength. The Boise sandstone samples failed by distributed cataclastic flow. The Bleurswiller sandstone samples failed by development of either discrete compaction bands (squares), or a hybrid mode of shear and compaction bands (circles).

collapse, whereas the compactive yield stress C^* marks the onset of shear-enhanced compaction [*Wong et al.*, 1997].

[11] Our mechanical data are compared with those for 1 hydrostatically and 8 triaxially compressed samples of Bleurswiller sandstone, previously presented by *Tembe et al.* [2008]. The critical stresses C^* and P^* for the two sandstones are compiled in Table S2, and compared in Figure 2b. The compactive yield stresses of Bleurswiller and Boise sandstones map out yield caps typical of a porous sandstone, with differential stress decreasing as a function of increasing mean stress. Furthermore, the yield stress levels for these two sandstones of similar composition and porosity are very similar, with caps almost coinciding each other.

5. Microstructural Observation

[12] Exterior appearances of samples of Boise and Bleurswiller sandstones that showed shear-enhanced compaction indicate fundamental differences in their failure modes (Table S2). Whereas discrete compaction bands and conjugate shear bands were observed in Bleurswiller sandstone, strain localization seemed to be absent in all of our Boise sandstone samples. Five of the failed samples of Boise sandstone that had undergone compactant failure were impregnated with epoxy and then sawed along a plane parallel to the axial direction to prepare petrographic thin-sections.

[13] To investigate the related microstructural evolution, we conducted systematic scanning electron microscope observations. Our observations on samples deformed by *Tembe et al.* [2008] elucidated the microstructural development of compaction localization in Bleurswiller sandstone. A compaction band ~1 mm wide can be seen near the mid-section of Figure 3, for a sample deformed at P_{eff} = 40 MPa to a maximum axial strain of 3.8%. Pervasive grain crushing had basically eliminated all the larger pores within the band, whereas grains and pores above and below remain relatively intact.

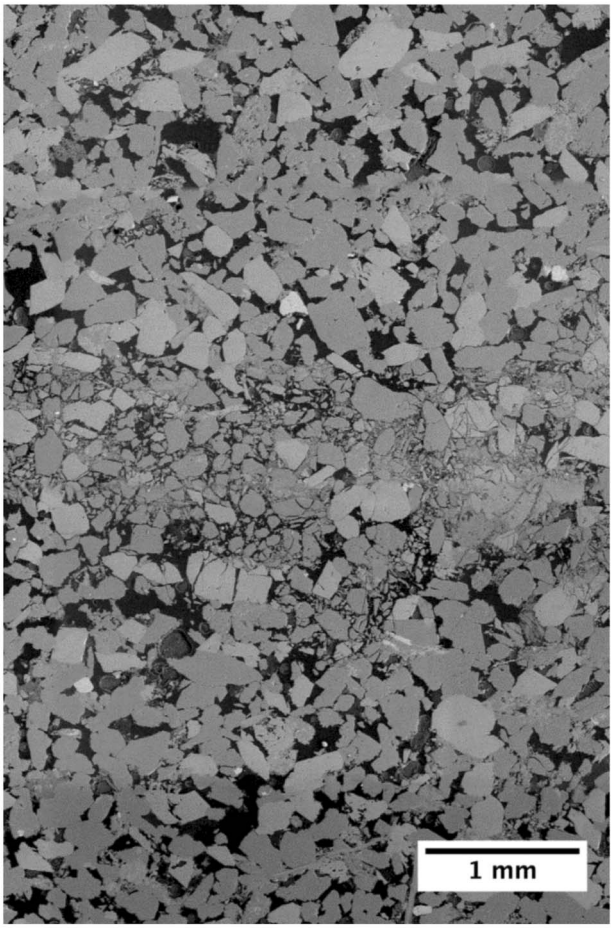

Figure 3. Backscattered scanning electron micrograph of discrete compaction band in Bleurswiller sandstone BL3 that was triaxially compressed (P_{eff} = 40 MPa) to 3.8% axial strain. The compaction band is about 1 mm wide and there is a clear absence of porosity pockets (in black) within this region. The direction of σ_1 is in vertical.

(a)

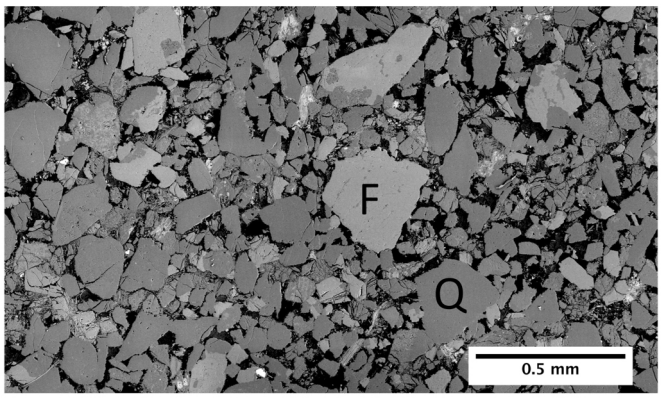

(b)

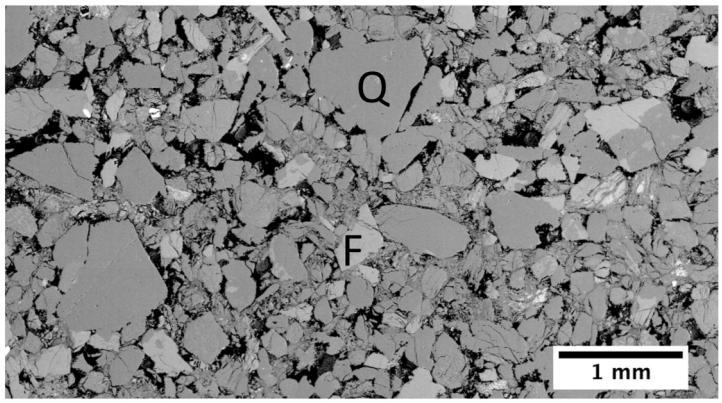

Figure 4. Backscattered scanning electron micrographs of Boise sandstone samples that were triaxially compressed (P_{eff} = 60 MPa) to axial strains of (a) 3.2% (BS15), and (b) 8.3% (BS21). Porosity pockets are distributed throughout the sample. Intense microcracking had developed in smaller grains, whereas the larger grains remain basically undamaged. These large intact grain, including both quartz (Q) and feldspars (F), have acted as barriers for propagation of damage. Note that there is progressive grain crushing in the smaller grains with increasing axial strain, however, the large grains still remained basically intact even in the more deformed sample BS21. The direction of σ_1 is in vertical.

[14] For comparison, we show typical damage observed in Boise sandstone sample BS15 (Figure 4a) deformed at P_{eff} = 60 MPa to an axial strain of 3.2%. Whereas intense microcracking had developed in smaller grains, larger grains remain basically undamaged. Although larger pores seem to be absent within a region in the lower left, many remain distributed over other areas. Sample BS21 was deformed to a significantly higher strain of 8.3% (Figure 4b). Pervasive crushing of the smaller grains was observed. Nevertheless, larger pores remain distributed throughout the sample. Although isolated Hertzian fractures had nucleated from impinging grain contacts, the larger grains remain basically intact, effectively acting as barriers for the coalescence of cataclastic damage to develop a percolative compaction band. The activation of these processes appears to be independent of the mineralogical composition, since larger intact grains of both quartz and feldspars were observed. The scenarios in all other Boise sandstone samples that underwent compactant failure were qualitatively similar. Accordingly, compaction localization was inhibited in this poorly sorted sandstone which failed by distributed cataclastic flow, although its compactive yield stresses were similar to Bleurswiller sandstone.

6. Discussion

[15] By a systematic comparison of the mechanical deformation and damage evolution in two sandstones of similar porosity and composition but different sorting, we clarified the micromechanical process by which grain size distribution controls compaction localization. Whereas previous studies focused on how compaction bands develop, our observations on Boise sandstone have elucidated the micromechanical process that inhibits their development in a poorly sorted rock. The process seems analogous to the "constrained comminution" model formulated by *Sammis et al.* [1987], who argued that the distribution of contact force in a granular assembly is such that the smaller grains can cushion the larger particles and shield them from being subjected to tensile stress concentration. Accordingly, the failure probability depends largely on the relative size of surrounding grains, such that the nearest neighbors of comparable size are more vulnerable to failure. As a result,

crushing would preferentially develop in the smaller grains while the larger grains remained intact, with the particle sizes converging to a fractal distribution. This scenario has recently been captured by 3D discrete element modeling [*Abe and Mair*, 2005].

[16] In agreement with numerical simulations of *Wang et al.* [2008], we observed that discrete compaction bands preferentially develop in a sandstone with relatively uniform grain size distribution (Figure 1a). The micromechanics of compaction localization in such a well sorted sandstone can be interpreted by the heuristic 2D model of *Wang et al.* [2008], who argued that the local stress perturbation due to pore collapse is similar to that of a square inclusion (with the two diagonals aligned with σ_1 and σ_3) subject to an isotropic transformational strain [*Eshelby*, 1957]. Their analytic results show that in the vicinity of the two corners along the diagonal aligned with σ_3, the stress perturbation is given by a tensor with the axial and transverse principal components given by $\Delta\sigma_1 = \Delta\sigma$ and $\Delta\sigma_3 = -\Delta\sigma$, with $|\Delta\sigma| \sim 200$ MPa. Such a significant enhancement of the local principal stress σ_1 would trigger further grain crushing and pore collapse near these two corners, leading to progressive propagation of compactant damage along an elongated zone perpendicular to σ_1.

[17] Figures 1a and 1c show that relatively narrow grain size distributions are associated with sandstones that develop compaction bands in the field and laboratory studies. Navajo sandstone has significantly coarser grains than Aztec, and yet pure compaction bands were observed in both field areas, indicating that their development is insensitive to the overall grain size. In Navajo sandstone, *Schultz et al.* [2010] observed that unlike layers 2 and 4 (Figure 1c), pure compaction bands were inhibited in the other three layers (1, 3 and 5) which are more porous and poorly sorted. Furthermore, it should be noted that unlike a laboratory test in which one can control the stress state, whether compaction bands can develop in a sandstone formation with appropriate microstructural attributes hinges on the attainment of the critical level of stress in the tectonic setting [*Eichhubl et al.*, 2010; *Fossen et al.*, 2011]. It is possible that microstructural attributes such as cementation and grain shape may also influence the mode of strain localization. Nevertheless, this laboratory study together with numerical simulations and field observations have demonstrated that like porosity, grain size distribution is a key petrophysical attribute that controls the development of compaction localization in a porous sandstone.

[18] **Acknowledgments.** We are grateful to Peter Eichhubl and Rich Schultz who kindly provided micrographs and data for Aztec and Navajo sandstones, respectively. We would also like to thank Peter Eichhubl for leading them on a most informative field trip to Valley of Fire. The research at Stony Brook was partially supported by the Office of Basic Energy Sciences, Department of Energy under grant DE-FG02-99ER14996 and DE-FG02-10ER16159. The authors would like to thank Peter Eichhubl, John Rudnicki and an anonymous reviewer for constructive comments on the paper.

[19] The Editor thanks Peter Eichhubl and two anonymous reviewers for their assistance in evaluating this paper.

References

Abe, S., and K. Mair (2005), Grain fracture in 3D numerical simulations of granular shear, *Geophys. Res. Lett.*, *32*, L05305, doi:10.1029/2004GL022123.

Aydin, A., R. I. Borja, and P. Eichhubl (2006), Geological and mathematical framework for failure modes in granular rock, *J. Struct. Geol.*, *28*, 83–98, doi:10.1016/j.jsg.2005.07.008.

Baud, P., E. Klein, and T. Wong (2004), Compaction localization in porous sandstones: spatial evolution of damage and acoustic emission activity, *J. Struct. Geol.*, *26*, 603–624, doi:10.1016/j.jsg.2003.09.002.

Baud, P., P. Meredith, and E. Townend (2012), Permeability evolution during triaxial compaction of an anisotropic porous sandstone, *J. Geophys. Res.*, *117*, B05203, doi:10.1029/2012JB009176.

Eichhubl, P., J. N. Hooker, and S. E. Laubach (2010), Pure and shear-enhanced compaction bands in Aztec Sandstone, *J. Struct. Geol.*, *32*, 1873–1886, doi:10.1016/j.jsg.2010.02.004.

Eshelby, J. D. (1957), The determination of the elastic field of an ellipsoidal inclusion and related problems, *Proc. R. Soc. London, Ser. A*, *241*, 376–396, doi:10.1098/rspa.1957.0133.

Fortin, J., S. Stanchits, G. Dresen, and Y. Guéguen (2006), Acoustic emission and velocities associated with the formation of compaction bands in sandstone, *J. Geophys. Res.*, *111*, B10203, doi:10.1029/2005JB003854.

Fossen, H., R. A. Schultz, and A. Torabi (2011), Conditions and implications for compaction band formation in the Navajo sandstone, Utah, *J. Struct. Geol.*, *33*, 1477–1490, doi:10.1016/j.jsg.2011.08.001.

Hill, R. E. (1989), Analysis of deformation bands in the Valley of Fire State Park, Nevada, MS thesis, 68 pp., Univ. of Nev., Las Vegas.

Katsman, R., E. Aharonov, and H. Scher (2005), Numerical simulation of compaction bands in high porosity sedimentary rock, *Mech. Mater.*, *37*, 143–162, doi:10.1016/j.mechmat.2004.01.004.

Klein, E., P. Baud, T. Reuschlé, and T. Wong (2001), Mechanical behaviour and failure mode of Bentheim sandstone under triaxial compression, *Phys. Chem. Earth*, *26*, 21–25, doi:10.1016/S1464-1895(01)00017-5.

Mollema, P. N., and M. A. Antonellini (1996), Compaction bands: A structural analog for anti-mode I cracks in aeolian sandstone, *Tectonophysics*, *267*, 209–228, doi:10.1016/S0040-1951(96)00098-4.

Sammis, C., G. King, and R. Biegel (1987), The kinematics of gouge deformation, *Pure Appl. Geophys.*, *125*, 777–812, doi:10.1007/BF00878033.

Schultz, R. A., C. H. Okubo, and H. Fossen (2010), Porosity and grain size controls on compaction band formation in Jurassic Navajo Sandstone, *Geophys. Res. Lett.*, *37*, L22306, doi:10.1029/2010GL044909.

Sternlof, K. R., J. W. Rudnicki, and D. D. Pollard (2005), Anticrack inclusion model for compaction bands in sandstone, *J. Geophys. Res.*, *110*, B11403, doi:10.1029/2005JB003764.

Tembe, S., P. Baud, and T. Wong (2008), Stress conditions for the propagation of discrete compaction bands in porous sandstone, *J. Geophys. Res.*, *113*, B09409, doi:10.1029/2007JB005439.

Vajdova, V., P. Baud, and T. Wong (2004), Permeability evolution during localized deformation in Bentheim sandstone, *J. Geophys. Res.*, *109*, B10406, doi:10.1029/2003JB002942.

Wang, B., Y. Chen, and T. Wong (2008), A discrete element model for the development of compaction localization in granular rock, *J. Geophys. Res.*, *113*, B03202, doi:10.1029/2006JB004501.

Wong, T., C. David, and W. Zhu (1997), The transition from brittle faulting to cataclastic flow in porous sandstones: Mechanical deformation, *J. Geophys. Res.*, *102*, 3009–3025, doi:10.1029/96JB03281.

Wong, T., P. Baud, and E. Klein (2001), Localized failure modes in a compactant porous rock, *Geophys. Res. Lett.*, *28*, 2521–2524, doi:10.1029/2001GL012960.